Past achievements and future challenges in the development of three-dimensional photonic metamaterials

Costas M. Soukoulis[1,2]* and Martin Wegener[3]

Photonic metamaterials are man-made structures composed of tailored micro- or nanostructured metallodielectric subwavelength building blocks. This deceptively simple yet powerful concept allows the realization of many new and unusual optical properties, such as magnetism at optical frequencies, negative refractive index, large positive refractive index, zero reflection through impedance matching, perfect absorption, giant circular dichroism and enhanced nonlinear optical properties. Possible applications of metamaterials include ultrahigh-resolution imaging systems, compact polarization optics and cloaking devices. This Review describes recent progress in the fabrication of three-dimensional metamaterial structures and discusses some of the remaining challenges.

ntroduced around a decade ago, metamaterials represent a broad class of densely packed micro- or nanostructured building blocks that are much smaller than the wavelength of light[1–5]. The Mie-like resonances of these building blocks open the door to a world of new possibilities. In particular, magnetic dipole resonances can be produced by shrinking the size of macroscopic metallic electromagnets such that their resonances enter the optical regime. A paradigm example of this is the split-ring resonator (SRR)[6], in which an incident light field induces a circulating and oscillating electric current that generates a magnetic dipole moment normal to the ring. Naively, the SRR can be viewed as a half-wave antenna rolled into an almost-closed circle. This picture gives a resonance wavelength that is 2π times larger than the ring's diameter — a value not far from more detailed calculations that also account for plasmonic effects occurring when the operating frequency approaches the metal's plasma frequency, which gradually turns the antenna resonance into a Mie resonance. The magnetic dipole resonance of the SRR, together with its numerous variations, have reminded the optics community that light is an electromagnetic wave. Obtaining complete control over an electromagnetic wave inside a material requires independent control over both its electric and the magnetic field[1,2]. Recent achievements in the control of magnetic fields have therefore opened an area of optics that is still considered irrelevant throughout many optics textbooks. Such advances allow for impedance matching, which can be used to achieve zero reflection at a material interface for any refractive index. The refractive index can also become negative under such circumstances, which means that the phase velocity of light is opposite to the electromagnetic energy flow described by the Poynting vector (more specifically, the dot product of the two vectors is negative). In other structures, the refractive index can take exceptionally large positive values if the phase velocity is very small. A large difference in refractive index between the left- and right-handed circular polarizations of a light wave results in significant optical activity. Finally, realizing the concepts of transformation optics requires tailored and generally anisotropic magnetodielectric metamaterials.
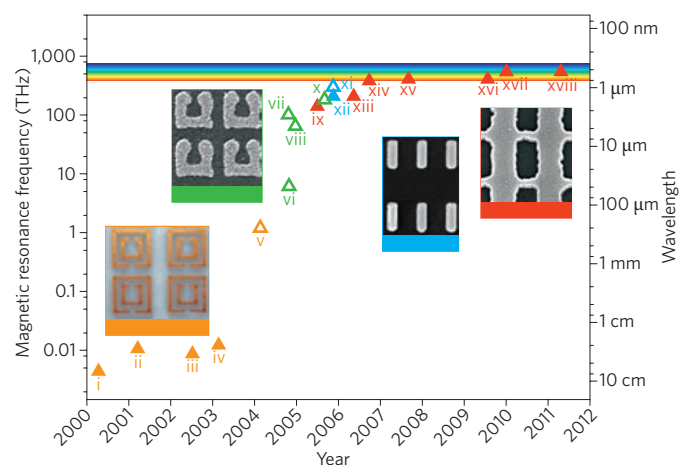

Figure 1 | Progress in metamaterial operating frequency over the past decade. The operating frequency of metamaterials with negative magnetic permeability μ (empty triangles) and negative index of refraction n (solid triangles) is shown on a logarithmic scale ranging from microwave to visible wavelengths. Orange: structures based on double SRRs; green: U-shaped SRRs; blue: metallic cut-wire pairs; red: negative-index double-fishnet structures. The four insets show optical or electron micrographs of the four types of structure. Data points are from: i) ref. 104; ii) ref. 20; iii) ref. 105; iv) ref. 106; v) ref. 107; vi) ref. 24; vii) ref. 108; viii) ref. 28; ix) ref. 7; x) ref. 109; xi) ref. 8; xii) ref. 9; xiii) ref. 10; xiv) ref. 11; xv) ref. 12; xvi) ref. 13; xvii) ref. 14; and xviii) ref. 15. Figure updated with permission from ref. 2, © 2007 AAAS.

There has never been a shortage of new ideas in the field of metamaterials. However, several conditions must be fulfilled before such ideas can make the transition from a curious scientific finding to a real-world usable material. First, the operating frequency must be brought to the optical regime, covering either

[1]Ames Laboratory and Department of Physics and Astronomy, Iowa State University, Ames, Iowa 50011, USA. [2]Institute of Electronic Structure and Laser, Foundation for Research and Technology-Hellas, 71110 Heraklion, Crete, Greece. [3]Institute of Applied Physics, Institute of Nanotechnology and DFG-Center for Functional Nanostructures, Karlsruhe Institute of Technology, D-76128 Karlsruhe, Germany. *e-mail: soukoulis@ameslab.gov
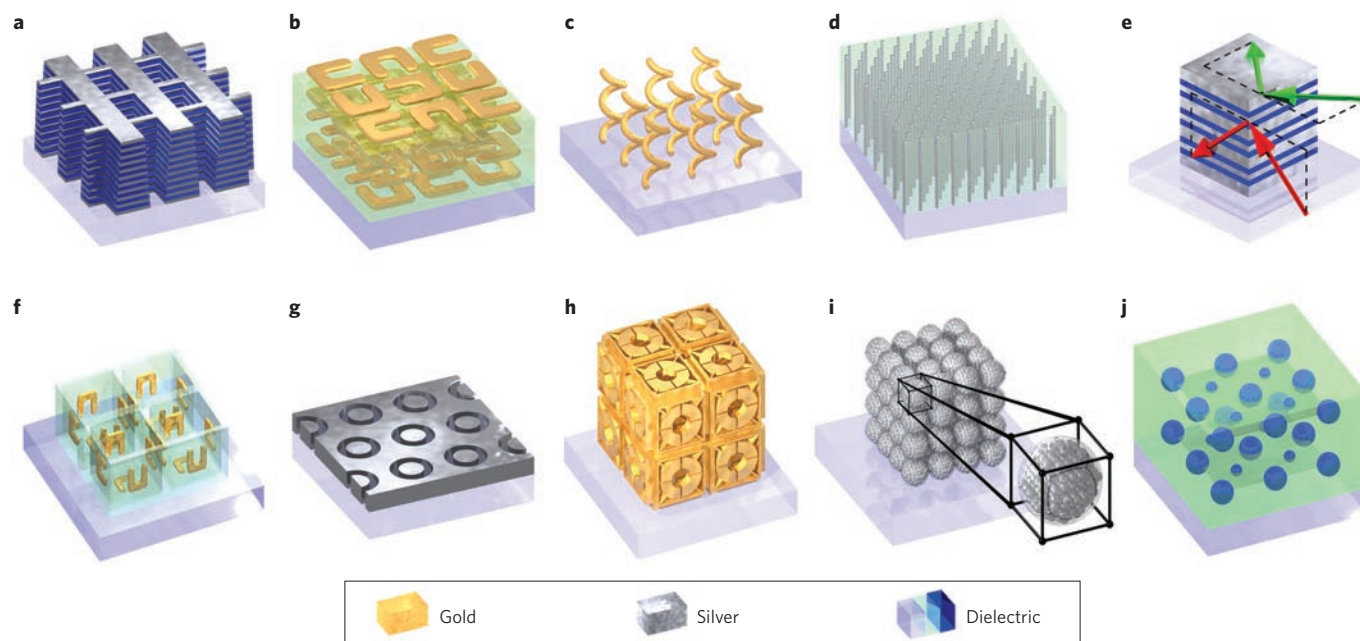
Figure 2 | 3D photonic-metamaterial structures. **a**, Double-fishnet negative-index metamaterial with several layers[13,15,19,22,27,71]. **b**, 'Stereo' or chiral metamaterial (see also Fig. 3) fabricated through stacked electron-beam lithography[24–26,29–33]. **c**, Chiral metamaterial made using direct-laser writing and electroplating[38]. **d**, Hyperbolic (or 'indefinite') metamaterial[43,45–50] made by electroplating hexagonal-hole-array templates[49]. **e**, Metal–dielectric layered metamaterial composed of coupled plasmonic waveguides, enabling angle-independent negative *n* for particular frequencies[44,45]. **f**, SRRs oriented in all three dimensions, fabricated using membrane projection lithography[51]. **g**, Wide-angle visible negative-index metamaterial based on a coaxial design[89]. **h**, Connected cubic-symmetry negative-index metamaterial structure amenable to direct laser writing[110]. **i**, Metal cluster-of-clusters visible-frequency magnetic metamaterial made using large-area self-assembly[79]. **j**, All-dielectric negative-index metamaterial composed of two sets of high-refractive-index dielectric spheres arranged on a simple-cubic lattice[52–55,65].

telecommunications or visible wavelengths (although there may also be applications at longer wavelengths). This condition was met a few years ago[1,2]. Second, to qualify as a 'material', the structures must have several layers of truly three-dimensional (3D) unit cells to approach the bulk 3D limit, which is the focus of this Review. Third, the losses (that is, absorption) should be reasonably low. Experimental progress in this direction has been sluggish for metal-based metamaterials[3–5], but all-dielectric structures avoiding metals may provide a solution in some frequency regimes.

Metamaterials go optical

In 2007 we reviewed how the operating frequency of magnetic and/or negative-index metamaterials has developed over the years[2]. Figure 1 is an updated version of these data. The tremendous increase in operating frequency has been made possible by miniaturizing and redesigning magnetic SRRs. Achieving negative refractive index also requires a negative electric permittivity, which is now provided by sets of long metal wires (known as a 'diluted metal') at both microwave and visible frequencies. This redesign process led to the development of the double-fishnet negative-index structure[7], which has been used in experiments by various groups[7–15]. In essence, a single functional layer of this structure comprises a perforated metal–dielectric–metal sandwich. The uniaxial double-fishnet structure exhibits an effective negative index of refraction for light propagating normal to the layers.

How can one provide experimental evidence that the index of refraction, *n*, is indeed negative? At optical frequencies, most groups merely measure the frequency dependence of the transmittance, *T*, and/or of the reflectance, *R*, and use computer simulations to fit the experimental values of *T* and *R*. The numerical results are then used to derive or 'retrieve'[16] the effective parameters of electric permittivity, ε, magnetic permeability, μ, and refractive index (and, more generally, also the bi-anisotropy parameter[17,18]). This simple retrieval approach can deliver reliable results provided that the agreement between experiment and theory is excellent. However, this approach is also quite indirect, and does not necessarily lead to unique results. For a single fishnet layer, the unit cell size along the propagation direction, a_z, is undefined. The phases of *T* and *R* change along a_z, but their magnitudes remain constant. As a_z decreases, the magnitude of the retrieved effective parameters tends to increase. In contrast, for two or more fishnet layers, the axial lattice constant a_z is well-defined and the retrieved results only depend on the number of layers. 'Bulk' metamaterial properties are reached if the retrieved parameters converge with an increasing number of layers (see discussion below). More directly, negative *n* should lead not only to negative refraction at the interface, but also to a negative phase velocity of light, and hence to a negative propagation time for phase fronts passing through a metamaterial slab. Researchers have demonstrated negative refraction at an interface by using a wedge prism at telecommunications wavelengths[19], in analogy to similar experiments at microwave frequencies[20]. However, caution is required in such cases because negative refraction can also occur without a negative refractive index[21]. Negative phase velocities of light have been investigated by directly measuring the phase and group propagation time of a Gaussian light pulse as it propagates through a thin metamaterial layer in an interferometric set-up[10,11]. Notably, a negative ('backwards') phase velocity can be accompanied by either a positive or negative group velocity, whereas the Poynting vector is always positive ('forwards')[10,11] (see Box 1).

Optical metamaterials go 3D

The next step[22] is to stack *N* > 1 functional layers of the double-fishnet structure (forming 2*N* + 1 layers in total) to achieve a bulk 3D uniaxial negative-index metamaterial (Fig. 2a). Table 1 summarizes the results of such experiments. The thickness of even the largest stack (*N* = 10) is still significantly smaller than the operating

Box 1 | Negative index of refraction

The term 'negative index of refraction' causes considerable confusion. First, one must specify whether the term refers to a negative phase index, n_p, or a negative group index, n_g. In both cases, 'negative' refers to the direction of the phase or group velocity vector with respect to the electromagnetic energy flow (Poynting vector **S**), which is tacitly assumed to be positive ('forwards'). Figure B1 illustrates these quantities for the simple case of an isotropic effective material with $\varepsilon(\omega) = \mu(\omega)$, such that no reflections occur at the interface between the material and vacuum or air.

Figure B1a shows the real and imaginary frequency dependence of the isotropic index of refraction $n(\omega)$. Figure B1b shows the wavevector **k** (**k'**), the group velocity vector $\mathbf{v}_g$ ($\mathbf{v}_g'$) and the Poynting vector **S** (**S'**) for the interface between air and the dispersive isotropic metamaterial. Figure B1c shows corresponding equifrequency surfaces for the dispersion relation $n(\omega)$. If the equifrequency contours move outwards with increasing frequency, then $\mathbf{v}_g \cdot \mathbf{k} > 0$; if they move inwards, $\mathbf{v}_g \cdot \mathbf{k}' < 0$. For the general case, $\mathbf{v}_p = (c/|n_p|)\hat{\mathbf{k}}$ and $\mathbf{v}_g = \nabla_k \omega = (c/|n_g|)\hat{\mathbf{k}}$, where c is the phase velocity of light in vacuum, $\hat{\mathbf{k}} = \mathbf{k}/|\mathbf{k}|$ and $n_g = \omega(d|n_p|/d\omega) + |n_p|$. It is also worth mentioning that $|\mathbf{k}| = \sqrt{(k_x^2 + k_y^2)} = R(\omega)$ and $|\mathbf{v}_p| = \omega/|\mathbf{k}| = c/|n_p|$, where $\omega = cR(\omega)/|n_p|$ and R is the radius of the circular equifrequency surface. The two middle diagrams shown in Fig. B1b are special cases, in which anomalous dispersion causes the energy flow **S** and the group velocity $\mathbf{v}_g$ to point in opposite directions. Causality still enforces the energy to flow away from the interface. This counter-direction of group velocity and energy flow is only possible because of the strong absorption associated with the anomalous dispersion region, which causes an incident pulse to eventually broaden and diminish in amplitude away from the interface. Within the anomalous dispersion region, the phase velocity may be either parallel or antiparallel to the energy flow or group velocity, resulting in either the positive or negative refraction of light. The anomalous dispersion region exists for arbitrarily small yet finite losses, and only disappears for the pathological case of zero loss. The negative group velocity corresponds to 'superluminal' pulse transmission; that is, the centre of a Gaussian pulse appears on the rear side of a slab before it enters the front side. However, this strange behaviour is not connected to the transfer of superluminal energy as a result of the inherent losses in this spectral region.

The concept of negative n_g is not new, and indeed it may be present in the anomalous dispersion region of any normal dielectric resonance (that is, $\mu = 1$) and many dielectric photonic crystals. A negative group index can lead to the negative refraction of light at an interface with air, even if the phase index is positive. Confusingly, a negative phase index also leads to negative refraction of light at an interface with air, even if the group index is positive. Negative refraction can also occur for birefringent dielectric materials with only positive phase and positive group indices. This confusion originates from the fact that Snell's law of refraction considers the angle of refraction of rays in geometrical optics, or the direction of the Poynting vector in wave optics. However, Snell's law generally makes no direct statement about the direction of the phase velocity vector. Thus, one must be very cautious when interpreting negative-refraction experiments.
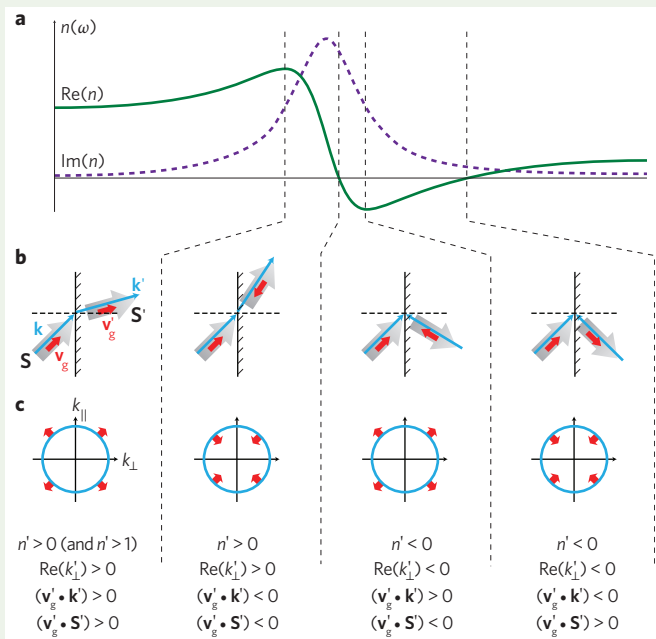

Figure B1 | Connection between the negative phase velocity of light and the negative refraction of light for the simple case of an isotropic effective medium with complex-valued frequency-dependent refractive index $n(\omega)$. a, Real and imaginary frequency dependence of the isotropic index of refraction, $n(\omega)$. **b**, The interface between air and the dispersive isotropic metamaterial, showing the wavevector **k**, the group velocity vector $\mathbf{v}_g$ and the Poynting vector **S**. **c**, The connection of **k**, $\mathbf{v}_g$ and **S** to the equifrequency surface (blue circle).

The phase refractive index $n_p = n$ is defined as $c = c_0/n$, where c is the phase velocity of light and c_0 is the speed of light in a vacuum. Thus, negative n immediately leads to negative phase velocity, which means that the optical path length becomes negative. Hence, the phase propagation time through a slab of thickness d also becomes negative. A negative phase propagation time, $\Delta t < 0$, can be measured in direct interferometric experiments. However, caution must be exerted when interpreting such experiments. Mathematically, a phase refractive index can be directly inferred through the relation $n = c_0 \Delta t/d$ (after appropriately separating effects due to the slab's surfaces). However, if the derived quantity n is a material property, it must only depend on the type of material and not on its thickness d. Thus, for example, if one doubles the slab's thickness, Δt must also double, leading to an identical value for n. A structure is a 'bulk metamaterial' if this condition is met, which is usually not the case for very thin metamaterial structures. The convergence from a single layer towards the bulk must be investigated for each metamaterial structure separately.

Much of the above discussion has tacitly assumed that the optical properties of the material/metamaterial under discussion are isotropic — a condition that is only rarely fulfilled in experiments. If this is not the case, the refractive index should be replaced by the appropriate tensor element.

---

wavelength. This raises the question: how many layers are sufficient for the material to qualify as '3D bulk'? The optical properties of a few-monolayer-thin SiO_2 film are not expected to be significantly different from those of a 50-nm-thick film, despite the fact that the total thickness is much smaller than one optical wavelength in both

cases (although the situation would be different if graphene were used instead of SiO_2). In metamaterials, the situation is more complex because the building blocks can strongly interact. One must therefore study how the effective optical parameters change as the number of layers increases. Thus, there is no single answer to the
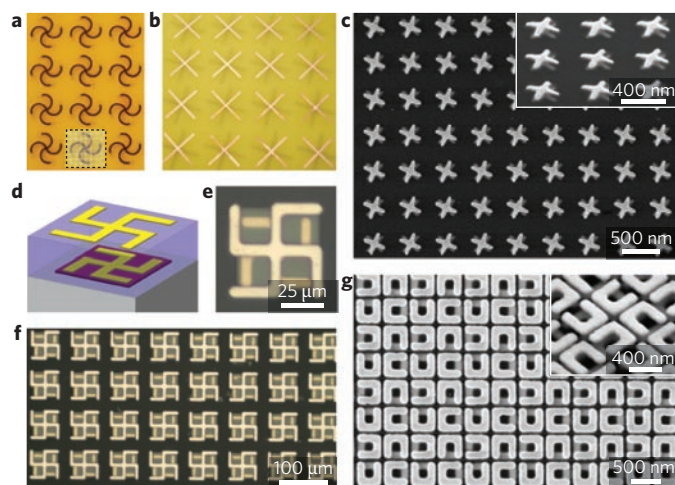
Figure 3 | 3D chiral metamaterials. a, Experimentally fabricated rosette chiral metamaterials that give negative *n* at gigahertz frequencies. **b**, Experimentally fabricated cross-wire chiral metamaterials that give negative *n* at gigahertz frequencies. **c**, Large-area electron micrograph of a chiral structure composed of right-handed twisted gold crosses, shown at normal and oblique (inset) angles. **d**, Schematic of the unit cell of a tunable chiral metamaterial. **e**, Top view of a single unit cell. **f**, Large-scale top view of a tunable chiral metamaterial. **g**, Electron micrographs of U-shaped SRRs. Figure reproduced with permission from: **a**, ref. 34 © 2009 APS; **b**, ref. 35 © 2009 APS; **c**, ref. 30 © 2009 OSA; **d–f**, ref. 33 © 2010 OSA; **g**, ref. 31 © 2010 OSA.

above question. In some cases, a single functional layer may be sufficient; in other cases, a few layers may be needed. The number of layers required to reach the bulk 3D regime strongly depends on the coupling between adjacent layers, and hence on the interlayer spacing. If the distance between adjacent functional layers is small, the coupling is strong, the convergence of the optical properties is slow, and at least four functional layers are required[23]. The behaviour converges, but not to that of the monolayer case. In contrast, for larger distances, the coupling is weak and the retrieved optical parameters for several functional layers are very similar to that of the monolayer case[23]. The retrieved effective parameters remain the same when increasing the number of layers, which means that the bulk metamaterial limit has been reached. The minimum number of layers required for the metamaterial to qualify as 'bulk' depends on both the structure under investigation and the choice of a_z. Several groups have fabricated multilayer SRRs, which give negative μ at both terahertz[24,25] and optical[26] frequencies.

The unit cell goes 3D

The double-fishnet structure shown in Fig. 2a is not only scientifically interesting but also relatively simple to fabricate, even for

Table 1 | Summary of fabricated double-fishnet negative-index metamaterials composed of *N* functional layers (or lattice constants) following a corresponding theoretical suggestion[22]. The structure is illustrated in Fig. 2a.

Number of functional layers	Reference	Year	Operating frequency
3	71	2007	214 THz
10	19	2008	166 THz
5	27	2008	188 THz
4	103	2008	1 THz
3	15	2011	439 THz

several functional layers. Standard electron-beam lithography[19,27], focused-ion-beam lithography[15,19], interference lithography[28] and nanoimprint lithography[29] have all successfully been used to fabricate double-fishnet designs, as well as a range of other metamaterial structures. However, there is more to making 3D metamaterials than simply adding more layers.

Flexibility in tailoring a metamaterial's unit cell interior is another crucial factor in metamaterial fabrication, especially when functionalities other than negative refractive index are desired. For example, strong chirality — a prerequisite for achieving large optical activity and circular dichroism — requires the lack of a mirror plane parallel to the substrate (for light incident normal to the surface), which is not possible with simple layered structures.

Stacked electron-beam lithography. Figure 2b shows a multilayer SRR structure that has been fabricated through stacked electron-beam lithography, a general stacking approach taken by several groups[24–27,29–33]. In this technique, a layer of unit cells is fabricated by electron-beam lithography and subsequent planarization. Planarization can, for example, be accomplished using a rather thick commercially available spin-on dielectric, which is then etched to a desired spacer thickness through reactive-ion etching. The next layer of unit cells is again fabricated using electron-beam lithography aligned with respect to the first layer. Using this technique, researchers have achieved lateral interlayer alignments down to the 10 nm level. Although in principle an unlimited number of layers can be fabricated, the structures demonstrated so far have all been restricted to only a small number, reaching a maximum of five[26].

Although stacked electron-beam lithography is already used to fabricate chiral structures with large circular dichroism and significant optical activity at optical frequencies[30,31], no negative refractive indices have been achieved at optical frequencies, in contrast with microwave[34–36] and far-infrared frequencies[32,33,37]. Figure 3 summarizes the development of chiral metamaterials[30–37] using this fabrication technique. In 2010, researchers experimentally fabricated tunable chiral metamaterials to exhibit tunable optical activity and tunable refractive indices for the first time[33].

Direct laser writing. The uniaxial gold helix metamaterial shown in Fig. 2c is another paradigm example of a chiral structure[38]. Like the planar SRR, 3D metal helices can be viewed as miniature electromagnetic coils into which a light field can induce an Ohmic current, giving rise to local magnetic dipole moments. Such structures have not been fabricated by any of the approaches mentioned above, and probably never will be. They can, however, be fabricated through direct laser writing (DLW), the 3D counterpart of 2D electron-beam lithography. In normal DLW, femtosecond laser pulses are tightly focused into the volume of a photoresist. Two-photon absorption ensures that only a tiny volume of the photoresist is sufficiently exposed by the light. Computer-controlled scanning of the focus and resist using piezoelectric actuators allows almost arbitrary polymer structures to be fabricated[39–41] with lateral resolutions of up to 100 nm. This value is an order of magnitude larger than state-of-the-art electron-beam lithography, which can readily access resolutions down to 10 nm. However, recent work using stimulated emission depletion DLW[42] has approached lateral resolutions of 50 nm, with potential for future improvements. The polymer structures produced through DLW lithography can be filled with gold using electroplating[38] (Fig. 2h). Electroplating setups can be extremely simple and inexpensive, often requiring only a bias voltage between a transparent electrode on the substrate and a macroscopic counter electrode within a beaker. The metamaterial sample footprint and height is therefore limited only by the DLW lithography process itself. For large-scale bulk samples,

DLW could be replaced by 3D interference lithography. However, to our knowledge this has not yet been achieved.

Other approaches for creating templates. Other metamaterial structures can be fabricated by filling anodized alumina templates with silver or gold, again using electroplating[38] (Fig. 2d). Although achieving isotropy remains a goal for some metamaterial structures, indefinite or hyperbolic metamaterials rely on intentional anisotropy[43]. Another technique for attaining negative refraction[44,45] is to use a metal–dielectric layered metamaterial (Fig. 2e). For electric fields parallel to either the metal wire axis (Fig. 2d) or the metallic layers (Fig. 2e), and for frequencies below the effective plasma frequency of the composite, the metamaterial's effective electric permittivity is negative, although it may be positive for the equivalent orthogonal polarization of light. The term 'hyperbolic metamaterial' originates from the hyperbolic shape of the isofrequency surfaces in wave-vector space[43]. These anisotropic systems can be used to achieve, for example, broadband all-angle negative refraction and superlens imaging[43–50]. Negative refraction and subwavelength imaging has been demonstrated at microwave[46], infrared[44,47] and visible wavelengths[49].

Membrane projection lithography. More complex designs (see Fig. 2f, for example) can be realized using the directional evaporation technique, which is also known as membrane projection lithography. This approach offers a path towards fabricating 3D metamaterials with micrometre-scale characteristic dimensions with arbitrary cavity shape and the ability to orient the SRR inclusions along each of the coordinate axes — a crucial step towards creating isotropic metamaterials. Along these lines, researchers at Sandia National Laboratories in the USA demonstrated[51] magnetic coupling to vertically oriented SRRs at operating wavelengths of 10 μm. Their experimental results are in good agreement with theoretical predictions. This novel technology is extremely flexible, but also technologically demanding. Although researchers have so far only demonstrated metamaterial structures with single functional layers, the approach in principle allows for multiple layers to be stacked.

Dielectric 3D optical metamaterials

All of the above metamaterials involve the use of metals, which leads to inherently large losses, particularly at optical or visible frequencies. It is interesting to ask, therefore, whether purely dielectric off-resonant (and hence low-loss) constitutive materials might also offer effective magnetic and/or negative-index metamaterials properties. The Mie resonances of dielectric particles play a key role[52] in achieving negative magnetic permeabilities[53–59], just as they do in metallic structures. It is known from Mie resonance theory that the first resonance of a dielectric sphere (and the second resonance of a cylinder) is a magnetic dipole mode. Its wavelength is controlled by the size and refractive index n_s of the sphere, which has diameter d. The condition $dn_s/\lambda_0 = (m + 1)/2$ determines the free-space wavelength λ_0 for the first magnetic resonance, where $m = 1$, as well as the first electric dipole resonance, where $m = 2$. To be used as a subwavelength building block in a metamaterial, the wavelength must be larger than the sphere diameter; for example, $\lambda_0/d > 10$. Further design freedom is provided if the set-up uses two sets of highly dielectric spheres made from the same dielectric material but of different radii, or two spheres of the same radius but different refractive indices. Such a structure is illustrated in Fig. 2j. For example, one set of spheres could offer electric dipole moments (leading to negative ε), whereas the other could provide magnetic dipole moments (negative μ). The inherently low losses of off-resonant dielectric materials cause the Mie resonances of metamaterials to be very narrow, which makes it difficult to overlap two sets of resonances. However, besides this

experimental difficulty, the realization of 3D isotropic negative-index metamaterials is relatively simple. Experiments have been performed at gigahertz[59] frequencies, where the sphere diameter is of the order of millimetres. In contrast, no corresponding experiments have yet been demonstrated at terahertz or even optical frequencies.

There are several alternative techniques for constructing 3D isotropic negative-index structures. First, the magnetic dipole resonances of dielectric spheres can be combined with off-resonant metal wires (see above; refs 60,61). Second, highly dielectric spheres embedded in a negative-permittivity plasmonic host such as a metal or a semiconductor[62] can be used. Third, highly dielectric spheres that provide negative μ can be coated with thin layers of a Drude metal of negative ε, which together lead to negative n at infrared frequencies[63–65]. Fourth, a 3D ensemble of polaritonic spheres for negative ε was proposed for achieving isotropic negative μ near the first Mie resonance at infrared frequencies[66–69]. Interestingly, both the magnetic and electric dipole resonances of highly dielectric spheres can survive in a random or non-periodic configuration[70], which enables the realization of low-loss 3D isotropic negative-index photonic metamaterials at infrared and optical frequencies.

Active loss compensation

Metamaterial losses become an increasingly important issue when moving from multiple metal-based metamaterial layers towards the bulk case. If, for example, the transmittance of a single metamaterial layer is as large as 90%, the transmittance of 100 layers is a mere $(0.9)^{100} \approx 3 \times 10^{-5}$, which renders the metamaterial essentially opaque and hence useless. The degree of loss can be quantified by a figure of merit (FOM), a dimensionless number that allows metamaterials operating in different wavelength regimes to be compared in a meaningful way. Mathematically, the FOM is connected to the complex-valued refractive index n by FOM = $|\text{Re}(n)/\text{Im}(n)|$. Over a length corresponding to one medium wavelength λ, the wave amplitude decays to $exp(-2\pi/\text{FOM})$. Equivalently, the $1/e$ intensity decay length is given by FOM × $\lambda/(4\pi)$. The best-measured values[15,71] of passive double-fishnet negative-index metamaterials have FOM = 3; that is, the $1/e$ intensity decay length is around a quarter of a wavelength inside the material. Such large losses are due to the fact that the region of negative n is very near to the resonance of the single unit cell, where $\text{Im}(n)$ is large. $\text{Im}(n)$, and hence any losses, can therefore be reduced by moving the region of negative n further away from the resonance. This can be accomplished in both the weakly and strongly coupled double-fishnet structures by introducing periodicity effects[23]. Although future design optimization might lead to small improvements, the desired increase of several orders of magnitude seems to be out of reach at optical frequencies.

An obvious way of compensating for loss is to introduce gain materials into the metamaterial structure. However, an FOM of 3 at wavelengths of 1 μm corresponds to an absorption coefficient of $\alpha \approx 4 \times 10^4$ cm^{-1}. Gain coefficients of this magnitude are difficult to obtain in practice[4]. However, recent experiments[72] on single layers of double-fishnet negative-index structures, in which the intermediate dielectric spacer layer was doped with dye molecules pumped by optical picosecond pulses, have raised hopes that solving this challenge, although difficult, may not be impossible. Corresponding theory[73,74] has also been published. Other experiments that exploit semiconductor gain in SRR metamaterials have only achieved partial loss compensation[75,76]. In principle, under stable steady-state conditions, the FOM can approach infinity at a single wavelength[77,78].

Conclusions and outlook

Over the past decade, electromagnetic metamaterials have come a long way from microwave to visible frequencies. More recently,

they have also become truly bulk 3D 'materials' at optical frequencies, albeit only for certain propagation directions and/or certain polarizations of light. However, none of these intricate 3D structures are yet available in quantities approaching the gram level. One future challenge is therefore to develop techniques for fabricating large-scale 3D isotropic metamaterials. As outlined above, some nanofabrication technologies have been developed specifically for this purpose, or have been modified from existing techniques. Electron-beam lithography, membrane projection lithography, direct laser writing, electroplating and bottom-up self-assembly approaches[79–81] are all examples of such techniques (see Fig. 2i).

Much of the research into photonic metamaterials has been inspired by the fascinating and far-reaching vision of the 'perfect lens', as introduced by John Pendry[82] — an idea based on the dream of lossless isotropic negative-index metamaterials. Although this dream may never come to fruition, it has already given birth to an entire field. Researchers have also identified short-term applications that exploit essentially 2D metamaterial structures. For example, metamaterial surfaces can even approach the realm of perfect absorption, where they neither transmit nor reflect light in a certain frequency regime for a broad range of angles[83–88]. Such compact perfect absorbers might prove useful for use as detectors or energy converters. Other researchers have explored field-enhancement effects for improving the performance of solar cells[89,90]. Sensitivity to magnetic fields is also required to achieve large chiral optical effects in 3D metamaterials, which enable the realization of compact broadband circular polarizers, for example[38]. At terahertz frequencies, using an array of conjugated bilayer metal resonators with photo-excitable semiconductor inclusions provides actively tunable optical activity with high transmission and very low polarization distortion[33]. Other short-term applications use metamaterials for sensing purposes by exploiting the dependence of their resonance peaks on the surrounding environment[91], or investigate nonlinear frequency conversion[6,92–98]. In addition, the metamaterial analogue of electromagnetically induced transparency[99–102] exhibits a transparency window that has extremely low absorption and strong adjustable dispersion. The latter could lead to 'slow-light' applications from microwave to terahertz frequencies, at which metamaterial structures can be fabricated quite easily. At optical frequencies, however, Ohmic losses impose fundamental constraints.

It is important to remember that the field of electromagnetic metamaterials is still rather young. After all, the first 'photonic' magnetic metamaterial structure emerged in November 2004 — around seven years ago. Since then, conceptual and technological progress in the field has been truly dramatic. However, the ultimate application of metamaterials — the one that solves a global challenge for mankind — remains to be identified. Using metamaterials to improve solar-energy harvesting or realize new medical diagnostic techniques are both prime candidates.

References

1. Shalaev, V. M. Optical negative-index metamaterials. *Nature Photon.* **1,** 41–48 (2007).
2. Soukoulis, C. M., Linden, S. & Wegener, M. Negative refractive index at optical wavelengths. *Science* **315,** 47–49 (2007).
3. Zheludev, N. I. The road ahead for metamaterials. *Science* **328,** 582–583 (2010).
4. Soukoulis, C. M. & Wegener, M. Optical metamaterials: More bulky and less lossy. *Science* **330,** 1633–1634 (2010).
5. Boltasseva, A. & Atwater, H. A. Low-loss plasmonic metamaterials. *Science* **331,** 290–291 (2011).
6. Pendry, J. B., Holden, A. J., Robbins, D. J. & Stewart, W. J. Magnetism from conductors and enhanced nonlinear phenomena. *IEEE T. Microw. Theory* **47,** 2075–2084 (1999).
7. Zhang, S. *et al.* Mid-infrared resonant magnetic nanostructures exhibiting a negative permeability. *Phys. Rev. Lett.* **94,** 037402 (2005).
8. Dolling, G., Enkrich, C., Wegener, M., Zhou, J. F. & Soukoulis, C. M. Cut-wire pairs and plate pairs as magnetic atoms for optical metamaterials. *Opt. Lett.* **30,** 3198–3200 (2005).
9. Shalaev, V. M. *et al.* Negative index of refraction in optical metamaterials. *Opt. Lett.* **30,** 3356–3358 (2005).
10. Dolling, G., Enkrich, C., Wegener, M., Soukoulis, C. M. & Linden, S. Simultaneous negative phase and group velocity of light in a metamaterial. *Science* **312,** 892–894 (2006).
11. Dolling, G., Wegener, M., Soukoulis, C. M. & Linden, S. Negative-index metamaterial at 780 nm wavelength. *Opt. Lett.* **32,** 53–55 (2007).
12. Chettiar, U. K. *et al.* Dual-band negative index metamaterial: Double negative at 813 nm and single negative at 772 nm. *Opt. Lett.* **32,** 1671–1673 (2007).
13. Garcia-Meca, C., Ortuno, R., Rodriguez-Fortuno, F. J., Marti, J. & Martinez, A. Double-negative polarization-independent fishnet metamaterial in the visible spectrum. *Opt. Lett.* **34,** 1603–1605 (2009).
14. Xiao, S. M., Chettiar, U. K., Kildishev, A. V., Drachev, V. P. & Shalaev, V. M. Yellow-light negative-index metamaterials. *Opt. Lett.* **34,** 3478–3480 (2009).
15. Garcia-Meca, C. *et al.* Low-loss multilayered metamaterial exhibiting a negative index of visible of refraction at visible wavelengths. *Phys. Rev. Lett.* **106,** 067402 (2011).
16. Smith, D. R., Schultz, S., Markos, P. & Soukoulis, C. M. Determination of effective permittivity and permeability of metamaterials from reflection and transmission coefficients. *Phys. Rev. B* **65,** 195104 (2002).
17. Kriegler, C. E., Rill, M. S., Linden, S. & Wegener, M. Bianisotropic photonic metamaterials. *IEEE J. Sel. Top. Quant.* **16,** 367–375 (2010).
18. Ku, Z. Y., Zhang, J. Y. & Brueck, S. R. J. Bi-anisotropy of multiple-layer fishnet negative-index metamaterials due to angled sidewalls. *Opt. Express* **17,** 6782–6789 (2009).
19. Valentine, J. *et al.* Three-dimensional optical metamaterial with a negative refractive index. *Nature* **455,** 376–379 (2008).
20. Shelby, R. A., Smith, D. R. & Schultz, S. Experimental verification of a negative index of refraction. *Science* **292,** 77–79 (2001).
21. Wegener, M., Dolling, G. & Linden, S. Plasmonics: Backward waves moving forward. *Nature Mater.* **6,** 475–476 (2007).
22. Zhang, S. A. *et al.* Optical negative-index bulk metamaterials consisting of 2D perforated metal-dielectric stacks. *Opt. Express* **14,** 6778–6787 (2006).
23. Zhou, J. F., Koschny, T., Kafesaki, M. & Soukoulis, C. M. Negative refractive index response of weakly and strongly coupled optical metamaterials. *Phys. Rev. B* **80,** 035109 (2009).
24. Katsarakis, N. *et al.* Magnetic response of split-ring resonators in the far infrared frequency regime. *Opt. Lett.* **30,** 1348–1350 (2005).
25. Miyamaru, F. *et al.* Three-dimensional bulk metamaterials operating in the terahertz range. *Appl. Phys. Lett.* **96,** 081105 (2010).
26. Liu, N. *et al.* Three-dimensional photonic metamaterials at optical frequencies. *Nature Mater.* **7,** 31–37 (2008).
27. Liu, N., Fu, L. W., Kaiser, S., Schweizer, H. & Giessen, H. Plasmonic building blocks for magnetic molecules in three-dimensional optical metamaterials. *Adv. Mater.* **20,** 3859–3865 (2008).
28. Zhang, S. *et al.* Experimental demonstration of near-infrared negative-index metamaterials. *Phys. Rev. Lett.* **95,** 137404 (2005).
29. Boltasseva, A. & Shalaev, V. M. Fabrication of optical negative-index metamaterials: Recent advances and outlook. *Metamaterials* **2,** 1–17 (2008).
30. Decker, M. *et al.* Strong optical activity from twisted-cross photonic metamaterials. *Opt. Lett.* **34,** 2501–2503 (2009).
31. Decker, M., Zhao, R., Soukoulis, C. M., Linden, S. & Wegener, M. Twisted split-ring-resonator photonic metamaterial with huge optical activity. *Opt. Lett.* **35,** 1593–1595 (2010).
32. Xiong, X. *et al.* Construction of a chiral metamaterial with a U-shaped resonator assembly. *Phys. Rev. B* **81,** 075119 (2010).
33. Zhou, J., Zhao, R., Soukoulis, C. M., Taylor, A. J. & O'Hara, J. Chiral THz metamaterial with tunable optical activity. *Proc. Conf. on Lasers and Electro-Optics* paper CTuF (2010).
34. Plum, E. *et al.* Metamaterial with negative index due to chirality. *Phys. Rev. B* **79,** 035407 (2009).
35. Zhou, J. F. *et al.* Negative refractive index due to chirality. *Phys. Rev. B* **79,** 121104 (2009).
36. Li, Z. F. *et al.* Chiral metamaterials with negative refractive index based on four 'U' split ring resonators. *Appl. Phys. Lett.* **97,** 081101 (2010).
37. Zhang, S. *et al.* Negative refractive index in chiral metamaterials. *Phys. Rev. Lett.* **102,** 023901 (2009).
38. Gansel, J. K. *et al.* Gold helix photonic metamaterial as broadband circular polarizer. *Science* **325,** 1513–1515 (2009).
39. Kawata, S., Sun, H. B., Tanaka, T. & Takada, K. Finer features for functional microdevices — micromachines can be created with higher resolution using two-photon absorption. *Nature* **412,** 697–698 (2001).
40. Deubel, M. *et al.* Direct laser writing of three-dimensional photonic-crystal templates for telecommunications. *Nature Mater.* **3,** 444–447 (2004).

41. Li, J. F., Hossain, M. D. M., Jia, B. H., Buso, D. & Gu, M. Three-dimensional hybrid photonic crystals merged with localized plasmon resonances. *Opt. Express* **18**, 4491–4498 (2010).

42. Fischer, J., von Freymann, G. & Wegener, M. The materials challenge in diffraction-unlimited direct-laser-writing optical lithography. *Adv. Mater.* **22**, 3578–3582 (2010).

43. Fang, A., Koschny, T. & Soukoulis, C. M. Optical anisotropic metamaterials: Negative refraction and focusing. *Phys. Rev. B* **79**, 241104 (2009).

44. Hoffman, A. J. *et al.* Negative refraction in semiconductor metamaterials. *Nature Mater.* **6**, 946–950 (2007).

45. Verhagen, E., de Waele, R., Kuipers, L. & Polman, A. Three-dimensional negative index of refraction at optical frequencies by coupling plasmonic waveguides. *Phys. Rev. Lett.* **105**, 223901 (2010).

46. Belov, P. A. *et al.* Transmission of images with subwavelength resolution to distances of several wavelengths in the microwave range. *Phys. Rev. B* **77**, 193108 (2008).

47. Casse, B. D. F. *et al.* Super-resolution imaging using a three-dimensional metamaterials nanolens. *Appl. Phys. Lett.* **96**, 023114 (2010).

48. Silveirinha, M. G., Belov, P. A. & Simovski, C. R. Ultimate limit of resolution of subwavelength imaging devices formed by metallic rods. *Opt. Lett.* **33**, 1726–1728 (2008).

49. Yao, J. *et al.* Optical negative refraction in bulk metamaterials of nanowires. *Science* **321**, 930–930 (2008).

50. Kawata, S., Ono, A. & Verma, P. Subwavelength colour imaging with a metallic nanolens. *Nature Photon.* **2**, 438–442 (2008).

51. Burckel, D. B. *et al.* Micrometer-scale cubic unit cell 3D metamaterial layers. *Adv. Mater.* **22**, 5053–5057 (2010).

52. Bohren, C. F. & Huffman, D. R. *Absorption and scattering of light by small particles.* (Wiley, 1983).

53. O'Brien, S. & Pendry, J. B. Photonic band-gap effects and magnetic activity in dielectric composites. *J. Phys. Condens. Mat.* **14**, 4035–4044 (2002).

54. Peng, L. *et al.* Experimental observation of left-handed behavior in an array of standard dielectric resonators. *Phys. Rev. Lett.* **98**, 157403 (2007).

55. Schuller, J. A., Zia, R., Taubner, T. & Brongersma, M. L. Dielectric metamaterials based on electric and magnetic resonances of silicon carbide particles. *Phys. Rev. Lett.* **99**, 107401 (2007).

56. Vynck, K. *et al.* All-dielectric rod-type metamaterials at optical frequencies. *Phys. Rev. Lett.* **102**, 133901 (2009).

57. Holloway, C. L., Kuester, E. F., Baker-Jarvis, J. & Kabos, P. A double negative (DNG) composite medium composed of magnetodielectric spherical particles embedded in a matrix. *IEEE T. Antenn. Propag.* **51**, 2596–2603 (2003).

58. Ahmadi, A. & Mosallaei, H. Physical configuration and performance modeling of all-dielectric metamaterials. *Phys. Rev. B* **77**, 045104 (2008).

59. Cai, X., Zhu, R. & Hu, G. Experimental study of metamaterials based on dielectric resonators and wire frame. *Metamaterials* **2**, 220–226 (2008).

60. Zhao, Q. *et al.* Experimental demonstration of isotropic negative permeability in a three-dimensional dielectric composite. *Phys. Rev. Lett.* **101**, 027402 (2008).

61. Zhao, Q. *et al.* Tunable negative permeability in an isotropic dielectric composite. *Appl. Phys. Lett.* **92**, 051106 (2006).

62. Seo, B. J., Ueda, T., Itoh, T. & Fetterman, H. Isotropic left handed material at optical frequency with dielectric spheres embedded in negative permittivity medium. *Appl. Phys. Lett.* **88**, 161122 (2006).

63. Wheeler, M. S., Aitchison, J. S. & Mojahedi, M. Coated nonmagnetic spheres with a negative index of refraction at infrared frequencies. *Phys. Rev. B* **73**, 045105 (2006).

64. Zhao, Q., Zhou, J., Zhang, F. & Lippens, D. Mie resonance-based dielectric metamaterials. *Mater. Today* **12**, 60–69 (December 2009).

65. Fu, N. *et al.* Three-dimensional negative-refractive-index metamaterials based on all-dielectric coated spheres. Preprint at http://arxiv.org/abs/1004.4694 (2010).

66. Engheta, N., Salandrino, A. & Alu, A. Circuit elements at optical frequencies: Nanoinductors, nanocapacitors and nanoresistors. *Phys. Rev. Lett.* **95**, 095504 (2009).

67. Yannopapas, V. Artificial magnetism and negative refractive index in three-dimensional metamaterials of spherical particles at near-infrared and visible frequencies. *Appl. Phys. A* **87**, 259–264 (2007).

68. Vendik, I., Odit, M. & Kozlov, D. 3D metamaterial based on a regular array of resonant dielectric inclusions. *Radioengineering* **18**, 111–116 (2009).

69. Huang, K. C., Povinelli, M. L. & Joannopoulos, J. D. Negative effective permeability in polaritonic photonic crystals. *Appl. Phys. Lett.* **85**, 543–545 (2004).

70. Yannopapas, V. Negative refraction in random photonic alloys of polaritonic and plasmonic microspheres. *Phys. Rev. B* **75**, 035112 (2007).

71. Dolling, G., Wegener, M. & Linden, S. Realization of a three-functional-layer negative-index photonic metamaterial. *Opt. Lett.* **32**, 551–553 (2007).

72. Xiao, S. *et al.* Loss-free and active optical negative-index metamaterials. *Nature* **466**, 735–738 (2010).

73. Wuestner, S., Pusch, A., Tsakmakidis, K. L., Hamm, J. M. & Hess, O. Overcoming losses with gain in a negative refractive index metamaterial. *Phys. Rev. Lett.* **105**, 127401 (2010).

74. Fang, A., Koschny, Th. & Soukoulis, C. M. Self-consistent calculations of loss-compensated fishnet metamaterials. *Phys. Rev. B* **82**, 121102 (2010).

75. Plum, E., Fedotov, V. A., Kuo, P., Tsai, D. P. & Zheludev, N. I. Towards the lasing spaser: Controlling metamaterial optical response with semiconductor quantum dots. *Opt. Express* **17**, 8548–8551 (2009).

76. Meinzer, N. *et al.* Arrays of Ag split-ring resonators coupled to InGaAs single-quantum-well gain. *Opt. Express* **18**, 24140–24151 (2010).

77. Stockman, M. I. Criterion for negative refraction with low optical losses from a fundamental principle of causality. *Phys. Rev. Lett.* **98**, 177404 (2007).

78. Kinsler, P. & McCall, M. W. Causality-based criteria for a negative refractive index must be used with care. *Phys. Rev. Lett.* **101**, 167401 (2008).

79. Rockstuhl, C., Lederer, F., Etrich, C., Pertsch, T. & Scharf, T. Design of an artificial three-dimensional composite metamaterial with magnetic resonances in the visible range of the electromagnetic spectrum. *Phys. Rev. Lett.* **99**, 017401 (2007).

80. Whitesides, G. M. & Grzybowski, B. Self-assembly at all scales. *Science* **295**, 2418–2421 (2002).

81. Erb, R. M., Son, H. S., Samanta, B., Rotello, V. M. & Yellen, B. B. Magnetic assembly of colloidal superstructures with multipole symmetry. *Nature* **457**, 999–1002 (2009).

82. Pendry, J. B. Negative refraction makes a perfect lens. *Phys. Rev. Lett.* **85**, 3966–3969 (2000).

83. Landy, N. I., Sajuyigbe, S., Mock, J. J., Smith, D. R. & Padilla, W. J. Perfect metamaterial absorber. *Phys. Rev. Lett.* **100**, 207402 (2009).

84. Liu, X., Starr, T., Starr, A. F. & Padilla, W. J. Infrared spatial and frequency selective metamaterial with near-unity absorbance. *Phys. Rev. Lett.* **104**, 207403 (2010).

85. Liu, N., Mesch, M., Weiss, T., Hentschel, M. & Giessen, H. Infrared perfect absorber and its application as plasmonic sensor. *Nano Lett.* **10**, 2342–2348 (2010).

86. Avitzour, Y., Urzhumov, Y. A. & Shvets, G. Wide-angle infrared absorber based on a negative-index plasmonic metamaterial. *Phys. Rev. B* **79**, 045131 (2009).

87. Diem, M., Koschny, Th. & Soukoulis, C. M. Wide-angle perfect absorber/thermal emitter in the THz regime. *Phys. Rev. B* **79**, 033101 (2009).

88. Chen, H. T. *et al.* Antireflection coating using metamaterials and identification of its mechanism. *Phys. Rev. Lett.* **105**, 073901 (2010).

89. Burgos, S. P., de Waele, R., Polman, A. & Atwater, H. A. A single-layer wide-angle negative-index metamaterial at visible frequencies. *Nature Mater.* **9**, 407–412 (2010).

90. Atwater, H. A. & Polman, A. Plasmonics for improved photovoltaic devices. *Nature Mater.* **9**, 205–213 (2010).

91. Liu, N. *et al.* Planar metamaterial analogue of electromagnetically induced transparency for plasmonic sensing. *Nano Lett.* **10**, 1103–1107 (2010).

92. Klein, M. W., Enkrich, C., Wegener, M. & Linden, S. Second-harmonic generation from magnetic metamaterials. *Science* **313**, 502–504 (2006).

93. Klein, M. W., Wegener, M., Feth, N. & Linden, S. Experiments on second- and third-harmonic generation from magnetic metamaterials. *Opt. Express* **15**, 5238–5247 (2007).

94. Niesler, F. B. P. *et al.* Second-harmonic generation from split-ring resonators on a GaAs substrate. *Opt. Lett.* **34**, 1997–1999 (2009).

95. Pendry, J. B. Time reversal and negative refraction. *Science* **322**, 71–73 (2008).

96. Wang, B., Zhou, J., Koschny, Th. & Soukoulis, C. M. Nonlinear properties of split ring resonators. *Opt. Express* **16**, 16058–16063 (2008).

97. Katko, A. R. *et al.* Phase conjugation and negative refraction using nonlinear active metamaterials. *Phys. Rev. Lett.* **105**, 123905 (2010).

98. Wang, Z. *et al.* Harmonic image reconstruction assisted by a nonlinear metamaterial surface. *Phys. Rev. Lett.* **106**, 047402 (2011).

99. Zhang, S., Genov, D. A., Wang, Y., Liu, M. & Zhang, X. Plasmon-induced transparency in metamaterials. *Phys. Rev. Lett.* **101**, 047401 (2008).

100. Papasimakis, N., Fedotov, V. A., Zheludev, N. I. & Prosvirnin, S. L. Metamaterial analog of electromagnetically induced transparency. *Phys. Rev. Lett.* **101**, 253903 (2008).

101. Tassin, P., Zhang, L., Koschny, Th., Economou, E. N. & Soukoulis, C. M. Low-loss metamaterials based on classical electromagnetically induced transparency. *Phys. Rev. Lett.* **102**, 053901 (2009).

102. Zhang, L. *et al.* Large group delay in a microwave metamaterial analog of electromagnetically induced transparency. *Appl. Phys. Lett.* **97**, 241904 (2010).

103. Paul, O., Imhof, C., Reinhard, B., Zengerle, R. & Beigang, R. Negative index bulk metamaterial at terahertz frequencies. *Opt. Express* **16,** 6736–6744 (2008).

104. Smith, D. R., Padilla, W. J., Vier, D. C., Nemat-Nasser, S. C. & Schultz, S. Composite medium with simultaneously negative permeability and permittivity. *Phys. Rev. Lett.* **84,** 4184–4187 (2000).

105. Bayindir, M., Aydin, K., Ozbay, E., Markos, P. & Soukoulis, C. M. Transmission properties of composite metamaterials in free space. *Appl. Phys. Lett.* **81,** 120–122 (2002).

106. Greegor, R. B., Parazzoli, C. G., Li, K. & Tanielian, M. H. Origin of dissipative losses in negative index of refraction materials. *Appl. Phys. Lett.* **82,** 2356–2358 (2003).

107. Yen, T. J. *et al.* Terahertz magnetic response from artificial materials. *Science* **303,** 1494–1496 (2004).

108. Linden, S. *et al.* Magnetic response of metamaterials at 100 THz. *Science* **306,** 1351–1353 (2004).

109. Enrich, C. *et al.* Magnetic metamaterials at telecommunication and visible frequencies. *Phys. Rev. Lett.* **95,** 203901 (2005).

110. Guney, D. O., Koschny, T. & Soukoulis, C. M. Intra-connected three-dimensionally isotropic bulk negative index photonic metamaterial. *Opt. Express* **18,** 12348–12353 (2010).